

Multimodal Image-to-Image Translation via a Single Generative Adversarial Network

Shihua Huang, Cheng He, Ran Cheng

Abstract—Despite significant advances in image-to-image (I2I) translation with Generative Adversarial Networks (GANs) have been made, it remains challenging to effectively translate an image to a set of diverse images in multiple target domains using a pair of generator and discriminator. Existing multimodal I2I translation methods adopt multiple domain-specific content encoders for different domains, where each domain-specific content encoder is trained with images from the same domain only. Nevertheless, we argue that the content (domain-invariant) features should be learned from images among all the domains. Consequently, each domain-specific content encoder of existing schemes fails to extract the domain-invariant features efficiently. To address this issue, we present a flexible and general SoloGAN model for efficient multimodal I2I translation among multiple domains with unpaired data. In contrast to existing methods, the SoloGAN algorithm uses a single projection discriminator with an additional auxiliary classifier, and shares the encoder and generator for all domains. As such, the SoloGAN model can be trained effectively with images from all domains such that the domain-invariant content representation can be efficiently extracted. Qualitative and quantitative results over a wide range of datasets against several counterparts and variants of the SoloGAN model demonstrate the merits of the method, especially for the challenging I2I translation tasks, i.e., tasks that involve extreme shape variations or need to keep the complex backgrounds unchanged after translations. Furthermore, we demonstrate the contribution of each component using ablation studies.

Index Terms—Image-to-Image translation, generative adversarial network, image synthesis.

I. INTRODUCTION

Image-to-Image (I2I) translation aims to learn a function that changes the domain-specific part/style of a given image to the target while preserving its domain-invariant part/content [1], [2]. A variety of vision and graphics problems, e.g., semantic segmentation, object detection, and de-blur can be formulated as the I2I problems (Fig. 1(a)). The Generative Adversarial Networks (GANs) [3] have received extensive attention in recent years, and a number of GAN based methods have been developed for vision tasks, e.g., person re-identification [4], [5], super-resolution [6], [7], text-to-image synthesis [8], [9], facial attribute manipulating [10]–[12]. Significant advances have been made in the I2I translation tasks with the help of GANs [13]–[17]. Among them, Pix2Pix [13] trains a conditional GAN with paired training data for supervised I2I tasks. In contrast, some works attempt

to learn I2I translation without supervision [18]–[21]. For instance, the CycleGAN [20] method introduces the cycle consistency loss for unsupervised I2I translation.

Although much progress has been made, those methods are not able to translate a single image to a set of diverse images in a target domain, known as multimodal image translation [22]. Fig. 1(b) shows one example of the multimodal I2I translation task, where a horse is translated to a few zebras but with diverse appearances. To address this issue, a number of multimodal image translation algorithms have been proposed in recent years, e.g., MUNIT [1] and DRIT [2], where the main idea is to employ a pair of content and style encoders to embed an image from a specific domain into a domain-invariant space and a domain-specific space, and then use a generator to map the latent codes to diverse outputs in a target domain (Fig. 2(a)). However, those methods are less efficient since multiple pairs of content and style encoders, as well as GANs, are required for multimodal image translation among multiple domains. Furthermore, these approaches use different domain-specific content encoders to learn domain-invariant features for different domains and train the model of each domain using the images from the same domain independently. Nevertheless, the domain-invariant features should be learned from images from all the domains. As such, it is unlikely for these schemes to effectively translate objects of different scales with complex backgrounds. As a result, existing methods may fail to translate objects with diverse appearance but in the complex background (e.g., translation from a horse in the wild to a zebra and vice versa as shown in Fig. 3(b)), since the translation methods should be aware of the diverse backgrounds among different domains are also the domain-invariant components.

For effective multimodal image translation among multiple domains, we propose an unsupervised image translation method. A single content encoder is used to encode the domain-invariant features of all the images from multiple domains; the style encoder and generator are shared among different domains in a conditional manner. In addition, a projection discriminator [23] with an additional auxiliary classifier is constructed, instead of multiple discriminators.

Specifically, we use an image and its label as input to the style encoder for domain-specific representation extraction, and feed the latent codes along with the target labels to the generator for generating a set of diverse target images. The general framework of our proposed method, SoloGAN, is presented in Fig. 2(b), which is able to learn multimodal mappings among multiple domains using a single pair of generator and discriminator.

S. Huang, C. He, and R. Cheng are with the University Key Laboratory of Evolving Intelligent Systems of Guangdong Province, Department of Computer Science and Engineering, Southern University of Science and Technology, Shenzhen 518055, China. E-mail: shihuahuang95@gmail.com, chenghehust@gmail.com, ranchengcn@gmail.com (Corresponding author: Ran Cheng).

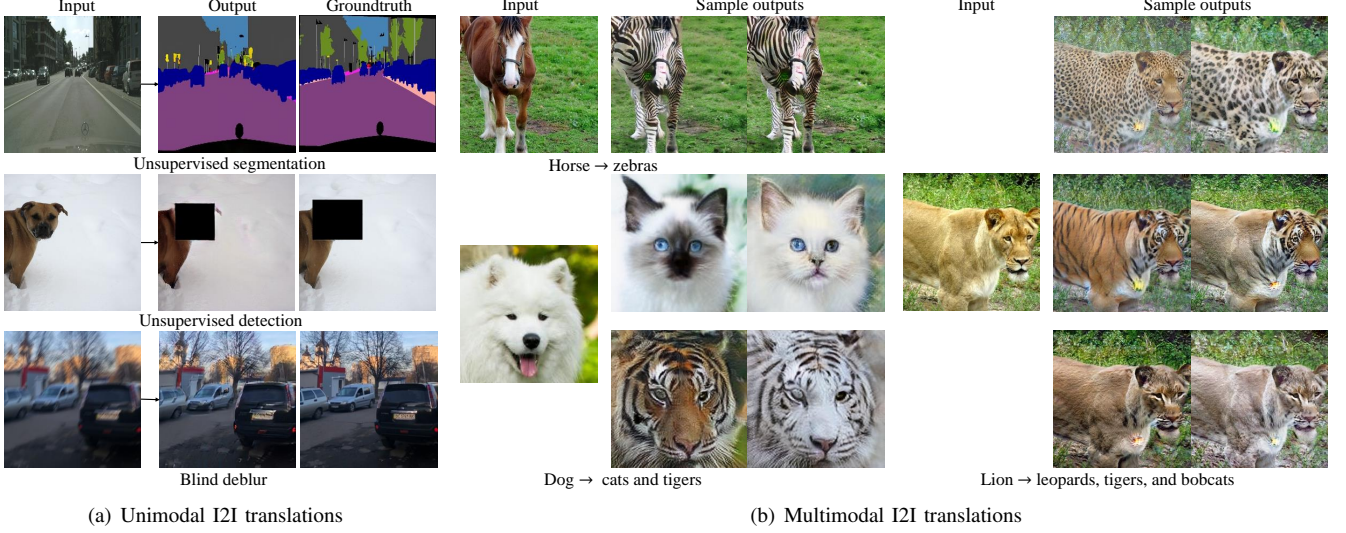


Fig. 1: Image-to-image translation results synthesized by (a) an unimodal variant of SoloGAN and (b) SoloGAN.

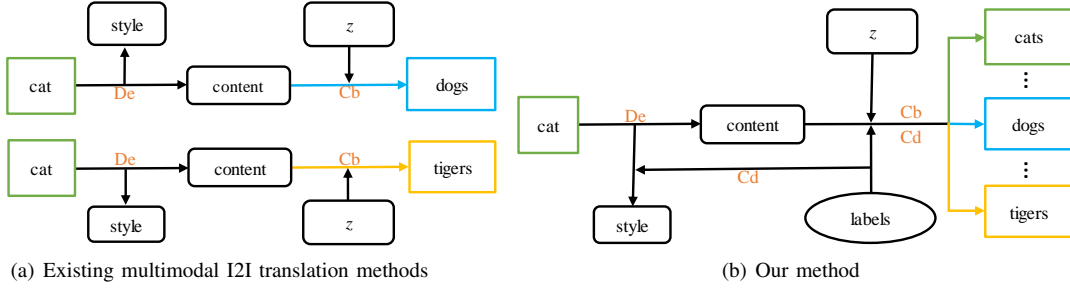


Fig. 2: Illustration of the workflows of existing multimodal I2I translation methods (a) and our method (b), where De, Cb, and Cd represent Decompose, Combine, and Condition, respectively. To translate an image from a source domain into a target domain, the latent space of the image is first decomposed into the content and style. A generator will combine the content and different style vectors (z , the random samples from $N(0, 1)$) to generate different target images. Taking the translation from the same cat into dogs and tigers as an example, existing methods need to decompose the cat twice and combine the content with different styles by using two different domain-specific encoders and generators, respectively. In contrast, our method can get objects of different domains with the same encoder and generator when given different target domain labels.

TABLE I: Comparisons of existing GAN-based image translation methods.

Method	Pix2Pix [13]	CycleGAN [20]	StarGAN [12]	BicycleGAN [22]	MUNIT [1]	DRIT [2]	SingleGAN [24]	SoloGAN
Unsupervised		✓	✓		✓	✓	✓	✓
MultiDomain			✓				✓	✓
MultiModal				✓	✓	✓	✓	✓
SinglePair			✓					✓

To better validate the performance of the proposed SoloGAN model, we modify existing datasets to be more challenging, where the images contain complex backgrounds or the translation of these images requires shape changes. Furthermore, we propose an evaluation method to assess the performance of I2I translation models more comprehensively. Since the failure of I2I models should be taken into consideration, the Fréchet Inception Distance (FID) [25] and classification error are adopted. Qualitative and quantitative comparisons against variants of SoloGAN and counterparts demonstrate the effectiveness of each component of SoloGAN and the merits of the whole method. The main contributions of this work are

summarized as follows:

- Different from existing multimodal image translation methods using multiple GANs, a single pair of generator and discriminator are adopted in the SoloGAN model efficiently.
- A projection model discriminator with an auxiliary classifier is proposed, which enables the SoloGAN model for effective multi-domain I2I translation.
- We provide more challenging datasets and propose an evaluation method for I2I translation. Qualitative and quantitative results demonstrate the efficiency and effectiveness of the SoloGAN model.

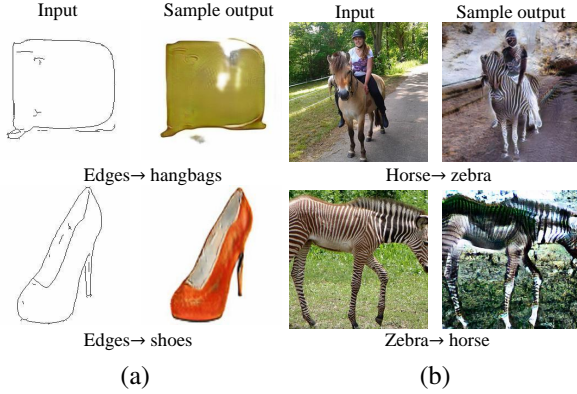


Fig. 3: (a) and (b) present images translation with simple and complex backgrounds achieved by MUNIT [1], respectively. MUNIT performs well in these simple backgrounds, but fails in these complex backgrounds.

II. RELATED WORK

A. Generative Adversarial Networks

Generative Adversarial Networks (GANs) [3] have gained much attention in recent years. To improve the training process as well as the quality and diversity of generated samples, some staple adversarial losses [26], [27] and regularization techniques [28], [29] have been proposed. In addition, conditional GANs [30] have been developed to help generate samples of desired classes. For instance, the ACGAN [31] method uses an auxiliary classifier to train the generator for generating samples of the desired classes. Image translation methods can be also formulated based on conditional GANs since the synthesized images belong to a specifically desired domain.

B. Image-to-Image Translation

The I2I translation task aims to learn a function to transfer the domain-specific part of a given image to the target domain [32]. In the Pix2Pix [13] method, a paired training dataset is used to train a cGAN [30] in a supervised manner. To alleviate the issues with collecting a large amount of paired training data, the CycleGAN [20] model uses a cycle consistency loss to preserve the key attributes between the input and the translated image. Despite demonstrated success, these methods have limited scalability in handling I2I translation among multiple domains, since different generative models should be trained for each pair of source/target domains. Instead of training multiple GANs for multi-domain I2I translation, e.g., ComboGAN [33], a number of methods explore multi-domain translation using a single GAN, e.g., StarGAN [12] and GANimation [11].

Numerous I2I translation problems are inherently multimodal. The BicycleGAN [22] model explicitly encourages a bijection between two spaces in a supervised manner, which makes it possible to generate different images using different latent codes. The MUNIT [1] and DRIT [2] methods are developed based on partially shared latent space, and use a content encoder as well as a style encoder to decompose the latent space of images into a domain-invariant part and a

domain-specific part, respectively. As a result, these methods are able to translate images while preserving the domain-invariant properties without supervision. Closely related to this work is the recently proposed SingleGAN [24] scheme which shares the style encoder and generator using a conditional approach. Nevertheless, the SingleGAN model still requires multiple discriminators to determine the domain of each image, and does not split the latent space into a domain-invariant and domain-specific parts. Table I shows the comparisons of existing I2I translation methods.

III. SOLOGAN

The goal of this work is to learn multimodal mappings among multiple domains using a single GAN. The overall network structure of our proposed SoloGAN is shown in Fig. 4(a), which consists of an encoder E (including a content E^c and a style E^s), a generator G and a discriminator D . Fig. 4(b) shows a sample of multimodal image-to-image translation among multiple domains by SoloGAN. In addition, the Central Biasing Instance Normalization (CBIN) [34] scheme is used for inductive bias.

A. Encoder

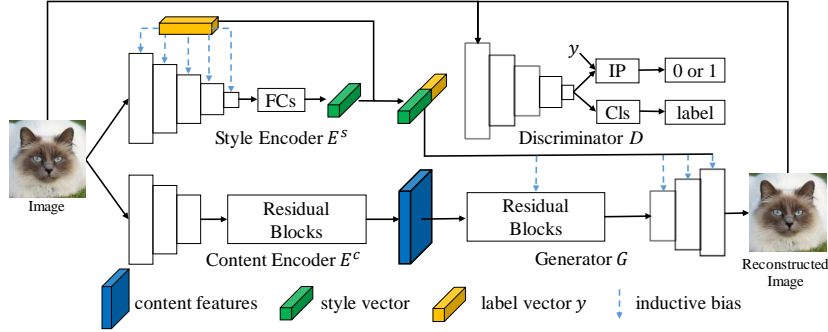
The encoder is used to map the input image into the latent space. As aforementioned, an image can be decomposed into the content as well as style in the latent space, and hence we design a content encoder and a style encoder, respectively. The content is domain-invariant that can be learned by a typical encoder, and the style is encoded using a conditional encoder with the domain labels being the condition (i.e., domain labels are transferred to one-hot vector). Furthermore, the style is distilled in a low-dimensional vector, where the length is set to 8 in this work.

B. Generator

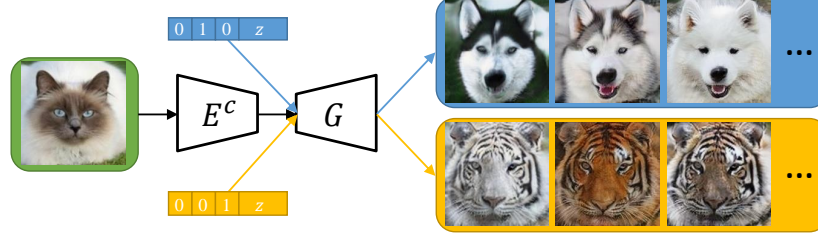
Conditioned by a target domain label, the generator in the SoloGAN model maps the given content and style to the output directly. Specifically, the target domain label vector is first concatenated with the given style vector, and fed into the generator network by using the CBIN scheme [34].

C. Discriminator

In contrast to the existing I2I methods that separate multiple domains into individuals and use multiple domain-specific discriminators to distinguish the target translated images, we use a single discriminator as in conventional class-conditional image generation [31], [35], [36]. Motivated by the classifier based discriminator [31] (Fig. 5(a)) and the projection discriminator (PD) [23] (Fig. 5(b)), we propose a new discriminator (as shown in Fig. 5(c)) in this work. The classifier based discriminator incorporates the label information into the objective function by augmenting the original discriminator objective with the likelihood score of the classifier on both the generated and training images. On the other hand, the projection operator incorporates the label into the discriminator by taking an inner product between the embedded one-hot vector

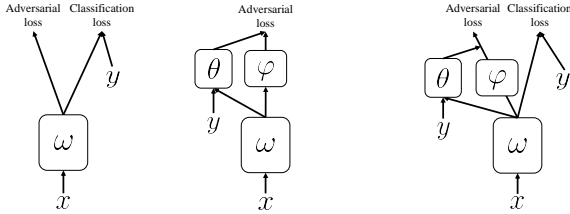


(a) Overall framework of SoloGAN



(b) Image translation condition on one-hot label vectors

Fig. 4: SoloGAN overview. The y is a domain label, where the label vector presented \mathbf{y} is the one-hot vector of y (e.g. given $y = 2$, $\mathbf{y} = (0, 0, 1)$), while FCs, IP, and Cls represent a few of fully connected layers, inner product operation, and a classifier, respectively. Both z represent style vectors sampling from $N(0, 1)$ randomly, while ‘010’ and ‘001’ are the one-hot label for dog and tiger, respectively.



(a) Classification (b) Projection (c) Projection with classification

Fig. 5: Three kinds of discriminator models for conditional GANs, where x and y are image and the label respectively, and ω , θ , and φ are learnable parameters.

domain label \mathbf{y} and the intermediate output feature vector, which significantly improves the quality of class conditional image generation. However, the projection discriminator is not effective in punishing the generator to translate the input image into a target domain. In the proposed projection with classification discriminator, a part of the projection model structure is shared with an auxiliary classifier, which helps the projection discriminator classify the translated images into a target domain. Instead of using multi-scale discriminators [37] as in most I2I GAN-based models (e.g., MUNIT [1] and DRIT [2]), we use a single-scale discriminator in this work.

D. Loss Functions

Adversarial loss. To make the images generated by our generator indistinguishable from the real images in the target

domains, we use the least-square adversarial loss [26]:

$$\begin{aligned} L_{adv}^D &= \mathbb{E}_{x,y',z \sim N(0,1)} [D(\hat{x})^2] + \mathbb{E}_x [(1 - D(x))^2], \\ L_{adv}^G &= \mathbb{E}_{x,y',z \sim N(0,1)} [(1 - D(\hat{x}))^2], \end{aligned} \quad (1)$$

where \hat{x} is an image in domain y' translated from x by $G(c, z, y')$, and c denotes the content extracted from x with E^c . Given an input pair (x, y) and a target domain label y' , the goal is to translate image x from domain y into domain y' . The generator G synthesizes an image \hat{x} conditioned on both the content of x (i.e. c) and target domain label y' , while the discriminator D aims to classify and distinguish between real and fake. We refer to the term $D(x)$ as a probability that an input x is a real sample in the domain y .

Domain classification loss. To force the generator to translate an input image into a target domain when conditioned by a target label, we use the domain classification loss of both real and translated images when optimizing D , G , and E :

$$\begin{aligned} L_{cls}^r &= \mathbb{E}_{x,y} [-\log D_{cls}(y|x)], \\ L_{cls}^t &= \mathbb{E}_{\hat{x},y'} [-\log D_{cls}(y'|\hat{x})], \end{aligned}$$

where L_{cls}^r and L_{cls}^t are used to optimize the D and the joint of G and E , respectively.

Cycle consistency loss. When there lack paired training samples for supervised learning, training G with respect to the adversarial loss in (1) does not guarantee that the translated images will preserve the content of the given image while only changing the style. To alleviate this problem, we apply a cycle consistency loss [20] to the generator:

$$L_{cyc} = \mathbb{E}_{x,y,\hat{x},y',s} [\|x - G(E^c(\hat{x}), s, y)\|_1],$$

TABLE II: Detailed structures of the proposed style and content encoder.

Input RGB image $x \in \mathbb{R}^{256 \times 256 \times 3}$	
CONV-(C64, K4x4, S2, P1)	CONV-(C64, K7x7, S1, P3), IN, ReLU
CD-ResBlock-(C128)	CONV-(C128, K4x4, S2, P1), IN, ReLU
CD-ResBlock-(C256)	CONV-(C256, K4x4, S2, P1), IN, ReLU
CD-ResBlock-(C256)	R-ResBlock-(C256)
CBIN, ReLU	R-ResBlock-(C256)
GAP	R-ResBlock-(C256)
FC-(8)	R-ResBlock-(C256)
Output $s \in \mathbb{R}^8$	Output $c \in \mathbb{R}^{64 \times 64 \times 256}$
Style Encoder	Content Encoder

where s denotes the style extracted from x with E^s . Note that c , \hat{x} (as given in (1)), and s are used as consistent denotations in the following unless otherwise specified. Specifically, an image x should be able to be reconstructed after being translated to \hat{x} within the target domain y' .

Bidirectional reconstruction loss. In order to encourage a bijection between two spaces, we introduce a bidirectional reconstruction loss as proposed in the MUNIT [1] method. When the generator maps the latent code of an image to the output, the output should be the same to the given image (image reconstruction), and an encoder should learn the mapping from the output back to the same latent code (latent reconstruction) with the following losses:

- **Image reconstruction.** The image reconstruction loss requires that the translated image could be reconstructed back to x by recombining its content and style:

$$L_{rec}^{img} = \mathbb{E}_{x,y,c,s} [\|x - G(c, s, y)\|_1].$$

- **Latent reconstruction.** The latent reconstruction is presented in the BicycleGAN [22] scheme for style reconstruction to alleviate the mode collapse problem. The MUNIT [1] method adds the content reconstruction loss to encourage the preservation of the semantic content in the input image during the translation with:

$$L_{rec}^{latent} = \mathbb{E}_{\hat{x}, y', z \sim N(0,1)} [\|z - E^s(\hat{x}, y')\|_1] + \mathbb{E}_{\hat{x}, c} [\|c - E^c(\hat{x})\|_1].$$

Full objective. We jointly train the pair of style and content encoder and generator while the discriminator is trained independently, and the final objective functions for the joint (L_{GE}) and discriminator (L_D) are:

$$L_{GE} = L_{adv}^G + \lambda_{cls} L_{cls}^t + \lambda_{cyc} L_{cyc} + \lambda_{rec}^{img} L_{rec}^{img} + \lambda_{rec}^{latent} L_{rec}^{latent},$$

$$L_D = L_{adv}^D + \lambda_{cls} L_{cls}^r,$$

where λ_{cls} , λ_{cyc} , λ_{rec}^{img} , and λ_{rec}^{latent} are hyper-parameters that control the relative importance of corresponding losses compared to the adversarial loss, which are set to 1, 10, 10, and 1 as suggested in prior work [1], [2], respectively.

IV. EXPERIMENTS

We first describe implementation details and introduce evaluation metrics as well as datasets in the experiments. The effectiveness of our model is validated by ablation studies and

TABLE III: Detailed structures of our proposed generator and discriminator. h is the output of global average pooling layer (GAP), d is the result from the fully connected layer given h as input, and n denotes the number of domains.

Input content $c \in \mathbb{R}^{64 \times 64 \times 256}$, style $s \in \mathbb{R}^8$		Input RGB image $x \in \mathbb{R}^{256 \times 256 \times 3}$	
CONV-(C256, K3x3, S1, P1), CBIN, ReLU		CONV-(C64, K4x4, S2, P1), LReLU	
C-ResBlock-(C256)		CONV-(C128, K4x4, S2, P1), LReLU	
C-ResBlock-(C256)		CONV-(C256, K4x4, S2, P1), LReLU	
C-ResBlock-(C256)		CONV-(C512, K4x4, S2, P1), LReLU	
C-ResBlock-(C256)		GAP	
C-ResBlock-(C256), CBIN, ReLU		FC-(1)	
TrCONV-(C128, K4x4, S2, P1), CBIN, ReLU		$dis = \text{Embed}(y) \cdot h + d$	
TrCONV-(C64, K4x4, S2, P1), CBIN, ReLU		CONV-(C1024, K4x4, S2, P1), LReLU	
CONV-(C3, K7x7, S1, P3), Tanh		$cls = \text{CONV}(\text{Cn}, K4x4, S1, P0)$	
Output RGB image $\hat{x} \in \mathbb{R}^{256 \times 256 \times 3}$		Output $dis \in \mathbb{R}^1$, $cls \in \mathbb{R}^n$	
Generator		Discriminator	

TABLE IV: Statistics of evaluated datasets.

Dataset	$cat \leftrightarrow dog \leftrightarrow tiger$				$black \leftrightarrow blond \leftrightarrow brown$			
	cat	dog	tiger		black	blond	brown	
Samples	train test train test	train test train test	train test train test		train test train test	train test train test	train test train test	
	771 100 1264 100	1173 100 5000 300	5000 300 5000 300		5000 300 5000 300	5000 300 5000 300	5000 300 5000 300	
Dataset	$summer \leftrightarrow winter$				$edges \leftrightarrow bags \leftrightarrow shoes$			
	summer	winter	edges		bags	edges	shoes	
Samples	train test train test	train test train test	train test train test		train test train test	train test train test	train test train test	
	1231 309 962 238	2500 150 2500 150	2500 150 2500 150		2500 150 2500 150	2500 150 2500 150	2500 150 2500 150	
Dataset	$horse \leftrightarrow zebra$				$leopard \leftrightarrow lion \leftrightarrow tiger \leftrightarrow bobcat$			
	horse	zebra	leopard		lion	tiger	bobcat	
Samples	train test train test	train test train test	train test train test		train test train test	train test train test	train test train test	
	1545 100 1070 100	620 100 919 100	777 100 530 100		530 100 530 100	530 100 530 100	530 100 530 100	
Dataset	$day \leftrightarrow night$				$photo \leftrightarrow Monet \leftrightarrow VanGogh \leftrightarrow Cezzan$			
	day	night	photo		Monet	VanGogh	Cezzan	
Samples	train test train test	train test train test	train test train test		train test train test	train test train test	train test train test	
	1000 100 993 100	1231 309 400 400	1072 121 525 58		525 58 525 58	525 58 525 58	525 58 525 58	

comparisons with other the state-of-the-art image translation methods. We then discuss limitations of the SoloGAN method.

A. Implementation Details

In this work, the Spectral Normalization (SN) [29] method is applied to the weights of the discriminator, generator as well as encoder in the training process, where the spectral norm of each layer is restricted. For all the experiments, the input image is of 256×256 pixels, and the Adam optimizer [38] with $\beta_1 = 0.5, \beta_2 = 0.999$ is used to train our model. Each mini-batch consists of one image from each domain. The Xavier initialization is used to assign the initial network weights of E, G , and D . The initial learning rate of E, G , and D is 0.0002 for the first n epochs, and it will decay to zero linearly in the rest n epochs, where n is set to 50 unless otherwise noted.

The network structures of the style encoder and content encoder are shown in Table II, and the structures of the generator as well as discriminator are shown in Table III. In the tables, C is the number of output channels, K is the kernel size, S is the stride size, P is the padding size, IN denotes the Instance Normalization, CBIN denotes the Central Biasing Instance Normalization, GAP is the Global Average Pooling layer, LReLU is the Leaky ReLU, and TrCONV is the Transposed CONVolution. The architectures of three different ResBlocks are shown in Fig. 6. The source code and trained models will be made available to the public.

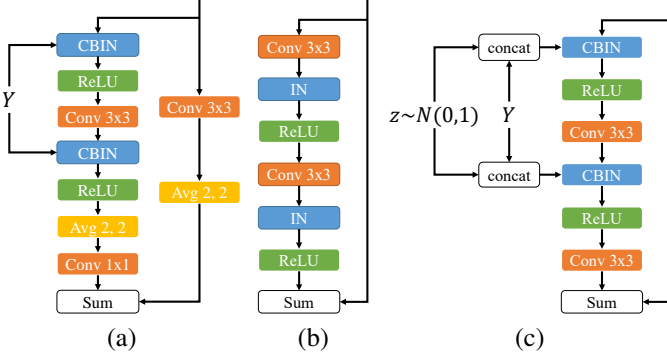


Fig. 6: (a) Conditional downsample residual block (CD-ResBlock) in our proposed style encoder where “Avg 2, 2” denotes an average pooling layer with both kernel and stride size set to 2. (b) Regular residual block (R-ResBlock) in our proposed content encoder. (c) Conditional residual block (C-ResBlock) used in our proposed generator.

B. Datasets

Table IV shows the datasets and statistics in the experiments. We briefly describe the properties of teach dataset below:

- *Day* \leftrightarrow *night*. The images are obtained from the Transient Attributes dataset [39] with different cloud patterns and lighting conditions.
- *Summer* \leftrightarrow *winter*. This dataset is used for translation of landscapes in summer and winter [20].
- *Edges* \leftrightarrow *bags&shoes*. This dataset is used to translate images between edges and real contents (i.e., handbags and shoes). A set of images are randomly sampled with equal probability from the edges2handbags and edges2shoes sets [13], which contain thousands of images of shoes and handbags.
- *Horse* \leftrightarrow *zebra* and *leopard* \leftrightarrow *lion* \leftrightarrow *tiger* \leftrightarrow *bobcat*. The images are obtained from the Animals With Attributes dataset [40]. These images contain objects at different scales across different backgrounds.
- *Cat* \leftrightarrow *dog* \leftrightarrow *tiger*. The dog and cat images are from [2] and the tiger pictures are collected by ourselves. The translation task among these domains needs to account for large shape changes.
- *Black* \leftrightarrow *blond* \leftrightarrow *brown*. This dataset is used to translate the color of human hair, which is randomly selected from the CeleA [41] dataset containing 202,599 face images with 40 attributes.
- *Photo* \leftrightarrow *VanGogh* \leftrightarrow *Monet* \leftrightarrow *Cezanne*. We extract images of the VanGogh, Monet, and Cezanne paintings from the photo2vangogh, photo2monet, and photo2cezanne datasets [20]. The summer images are from the summe2winter dataset [20].

C. Quantitative Evaluation Metrics

We present the metrics for quantitatively evaluating the quality and diversity of translated images.

Quality. The Inception Score (IS) [42] and Fréchet Inception Distance (FID) [25] are two widely-used metrics for measuring

the quality of the generated images by GANs. For IS, we use an Inception-V3 classifier [43] fine-tuned on our specific dataset and 10k translated images (100 input images and 100 translated samples per given input) are used to evaluate the IS. For FID, we use the ImageNet-pretrained Inception V3 [43] with 100 input images from each domain and 10 translated samples per given input. A lower FID value indicates a higher quality image whereas a higher IS score is better.

Diversity. For diversity assessment, we introduce the LPIPS distance [44], which is computed by the weighted L_2 distance between deep features of 19 paired images per given input. There are 100 different input images per domain, and the ImageNet-pretrained AlexNet [45] is used as the feature extractor. In addition, we introduce the Conditional Inception Score (CIS) [1], which is modified from IS to measure the diversity of outputs conditioned on a single input image. It is calculated as the IS but with a different estimated equation as given in [1]. A higher value of either IS or CIS indicates an image with wider diversity.

Classification error. Since the above evaluation metrics are not effective to explicitly reflect whether a translation is successful, we propose to compute the classification error of translated images as an additional performance metric. We use the above-mentioned finetuned Inception-V3 model, with a classification error of 0.50% on the test set, as a classifier. We then perform image translation on 100 test images for each domain, where 10 translated images given each test image are selected to make a new test set. Finally, we classify those images with annotated target domain labels. A lower classification error reflects the model has a higher success rate to translate input images into target domains.

User preference. We conduct a user study to evaluate the realism of translated images. We study $2 \times n$ input images for each translation task between two domains, e.g., n images of the cat are input for translation from the cat to the dog while n images of dog need to be translated to cats. In this work, we set n to 50, and choose *cat* \leftrightarrow *dog* as well as *horse* \leftrightarrow *zebra*. We use these two datasets since they are two representative translation tasks that need to account for large shape changes or maintain the complex background unchanged.

D. Evaluated Methods

Three variants of SoloGAN, i.e., w/o latent, w/o Cls, and w/o PD, are presented to validate the functionality of each component in the SoloGAN model. The first two variants ablate I_{rec}^{latent} and classifier respectively, and the third one replaces the projection model discriminator with a conventional discriminator.

We evaluate the proposed method against the StarGAN [12], MUNIT [1], DRIT [2] and SingleGAN [24] models. The StarGAN method is an unimodal model that addresses the issue of using multiple GANs for translation among multiple domains. The MUNIT and DRIT models focus on unsupervised multimodal image translation via disentangled representations, which consist of an encoder (i.e. style encoder as well as content encoder) and a GAN for each domain. Given a number

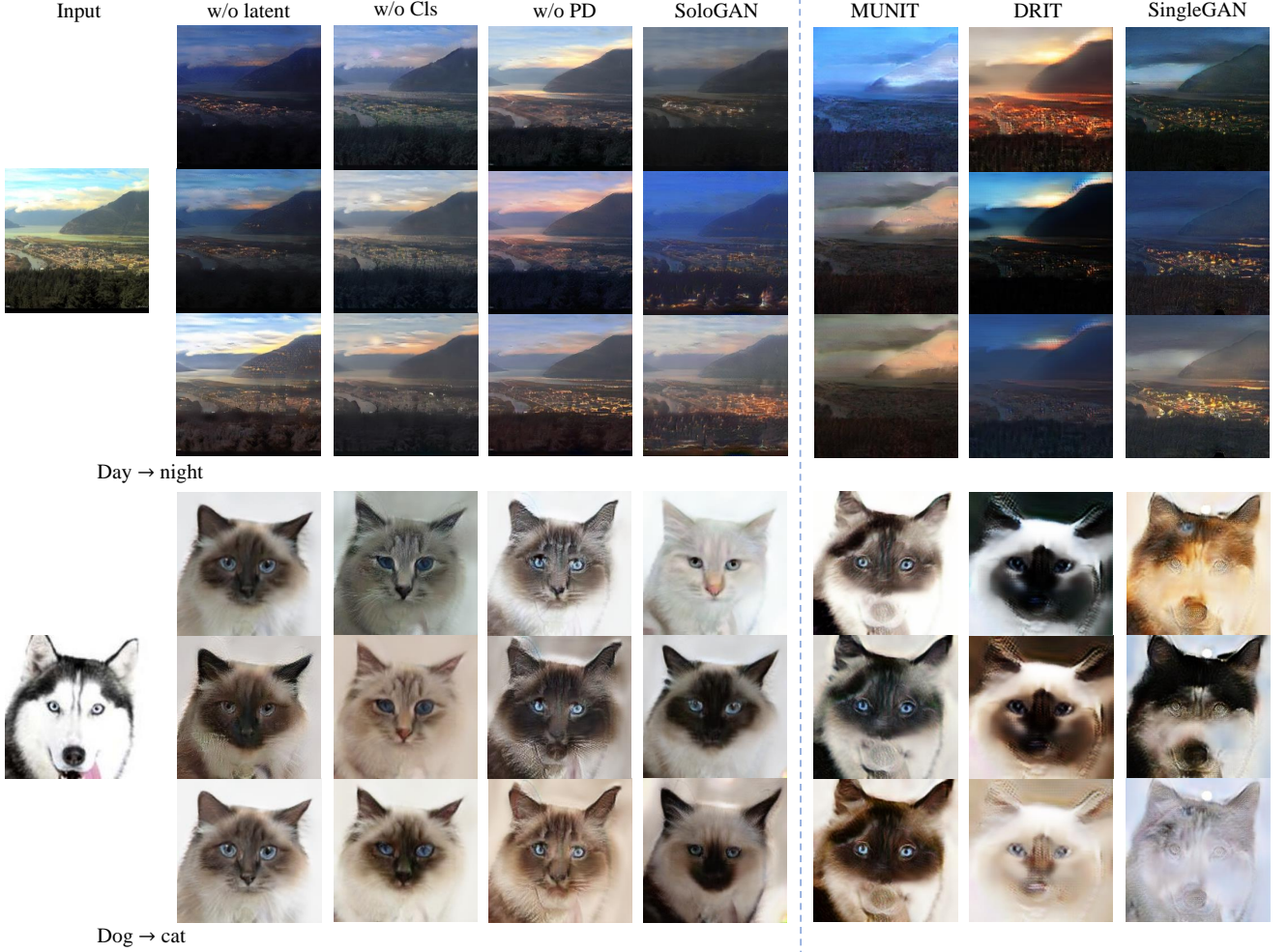


Fig. 7: Synthesized images by different multimodal I2I translation methods.

of n domains, both MUNIT and DRIT models need to train n encoders and GANs for image translation. The SingleGAN method shares the style encoder and generator using the domain labels as a condition, while multiple discriminators are required for distinguishing images in different domains. In contrast to the MUNIT, DRIT and SingleGAN methods which have all employed multi-scale discriminators, the proposed SoloGAN model adopts one single-scale discriminator.

E. Empirical Results

The $cat \leftrightarrow dog$ dataset is derived from $cat \leftrightarrow dog \leftrightarrow tiger$ database. For fair comparisons, we train all the evaluated methods for 100 epochs.

1) *Qualitative Evaluation*: Fig. 7 shows synthesized images by the SoloGAN, MUNIT, DRIT, SingleGAN, methods and three variants of the SoloGAN model on the $day \rightarrow night$ and $cat \leftarrow dog$ datasets. Fig. 8 shows additional results on the $cat \rightarrow dog$ and $horse \leftrightarrow zebra$ dataset synthesized by the SoloGAN, MUNIT, DRIT, and SingleGAN models. The generated results by the SoloGAN and StarGAN models for multi-domain translation are shown in Fig. 9 on the $tiger \rightarrow cat$, dog , and $bobcat \rightarrow leopard$, $lion$, $tiger$ datasets.

The SoloGAN method suffers from the partial mode collapse problem without L_{rec}^{latent} (w/o latent). Similarly, the SoloGAN is less effective in generating diverse and realistic images without the projection discriminator (w/o PD) or classifier (w/o Cls).

Overall, the proposed SoloGAN model performs well in translating images with wider diversity. In contrast, the other methods are less effective in image translation tasks that involve significant shape changes, e.g, translating dog to cat images. Meanwhile, the three evaluated methods are less effective in image translation on the $cat \rightarrow dog$ dataset. Although the other methods are able to translate horse into zebra images and vice versa, these schemes are less effective in retaining complex background than the proposed approach. Furthermore, the StarGAN model does not translate tiger to cat or dog images well (as an effective model needs to account for large shape changes in image translation). The SoloGAN algorithm performs significantly better on the $bobcat \rightarrow leopard$, lion and tiger dataset than the StarGAN model.

2) *Quantitative Evaluation*: Table V shows quantitative results of the evaluated methods. Without L_{rec}^{latent} , the LPIPS score of the SoloGAN model drops dramatically from 0.300 to

TABLE V: Quantitative results, where P and T represent the parameters of the generator (including encoder) and the run time when translating an input image to 100 images of a target domain, respectively.

Method	<i>day ↔ night</i>	<i>cat ↔ dog</i>				# P (M)	# T (s)
	LPIPS	Cls_error (%)	CIS	IS	FID		
SoloGAN	0.300	0.05	1.031	1.050	0.226	13.99	1.053
SoloGAN w/o latent	0.217	0.05	1.045	1.018	0.221	13.99	1.053
SoloGAN w/o Cls	0.253	0.40	1.028	1.062	0.244	13.99	1.053
SoloGAN w/o PD	0.254	0.50	1.074	1.030	0.304	13.99	1.053
MUNIT [1]	0.191	5.40	1.075	1.185	0.490	2×15.03	1.447
DRIT [2]	0.280	5.10	1.048	1.172	0.753	2×10.65	0.976
SingleGAN [24]	0.323	32.15	1.113	1.315	0.732	9.8	0.795

TABLE VI: Classification errors for multi-domain translation generated by SoloGAN and StarGAN. For fair comparisons, we sample one image randomly from the multimodal outputs obtained by SoloGAN given an input image.

Dataset	SoloGAN	StarGAN
<i>cat ↔ dog ↔ tiger</i>	0.83%	61.00%
<i>leopard ↔ lion ↔ tiger ↔ bobcat</i>	7.92%	58.75%

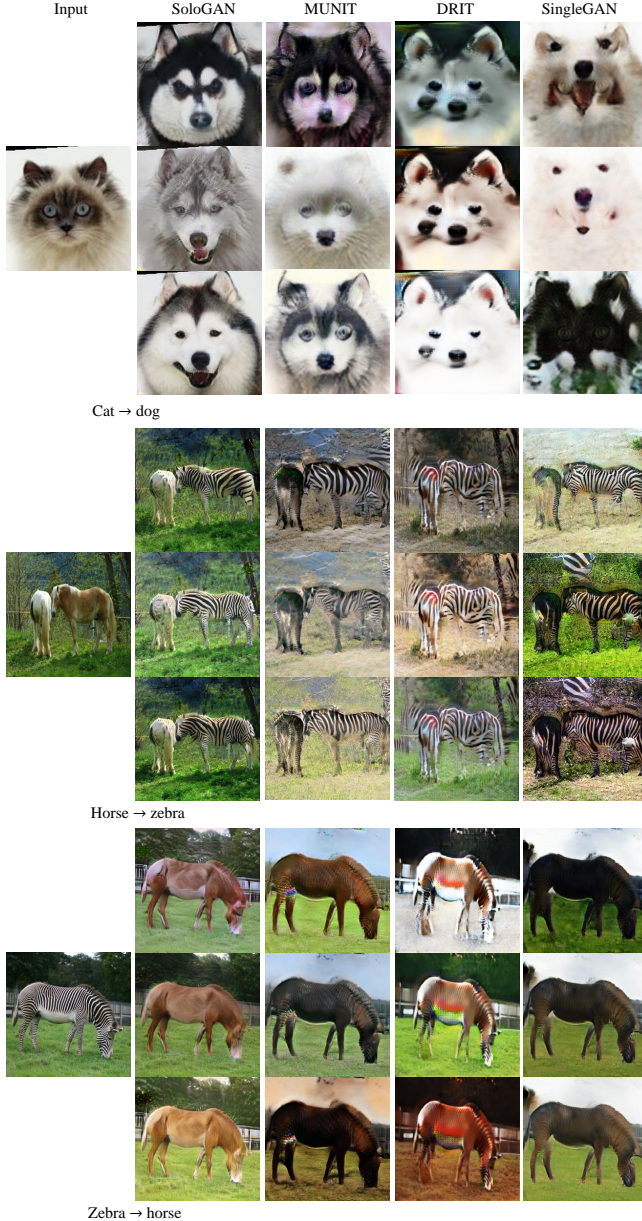


Fig. 8: More qualitative comparison samples on *cat → dog* and *horse ↔ zebra* translation tasks.

0.217. When using only the proposed classifier or projection discriminator, the SoloGAN method does not perform well in terms of the LPIPS, IS, and FID values. Furthermore, the classification errors achieved by these two variants are about 10 times as large as that generated by the proposed model. These results indicate the proposed components play important roles for translating images into target domains effectively.

As shown in Table V, the proposed SoloGAN model performs well in generating diverse images on *day ↔ night* dataset when compared with the SingleGAN method (0.300 vs 0.323), and outperforms the MUNIT and DRIT schemes. In terms of classification error, the SoloGAN model performs favorably against the evaluated schemes. We note that all the other methods achieve better IS scores but worse FIDs than the SoloGAN model on the *cat ↔ dog*. In addition, the FID scores of these methods are proportional to the classification errors. As the FID score is designed to compare the statistics of synthetic samples and real-world samples, it can be used to detect translation failures. We also evaluate all the translation methods in terms of parameters of the generator (including encoder) and the run time using a single Tesla V100. Different from the MUNIT and DRIT methods, the parameters of our model do not increase with the number of domains. Overall, the SoloGAN model performs efficiently and effectively against the evaluated methods.

Fig. 10 shows user study results where the results synthesized by the SoloGAN model are considered more realistic than those by the other schemes. Table VI shows classification errors of the StarGAN and SoloGAN methods for multi-domain image translation. The results show that the SoloGAN model is effective in handling unsupervised I2I translation among multiple domains in terms of both effectiveness and efficiency.

In addition to control over the translation output of desired target domains, our SoloGAN can provide example-guided image translation due to the disentangled representation of content and style vectors. Given a content image x_1 from domain y_1 and a style image x_2 of domain y_2 , our generator



Fig. 9: Synthesized images by different multi-domain I2I translation methods.

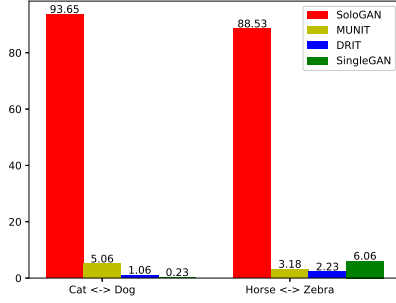


Fig. 10: User preference results collected from 100 reports, where the vertical axis indicates the percentage of preference.

produce an image \hat{x}_1 that recombines the content of x_1 and the style of x_2 by $G(E^c(x_1), E^s(x_2), y_2)$. Some example-guided translation results by the SoloGAN model are shown in Fig. 11, which demonstrate its success in disentangling contents and styles with the same content encoder and style encoder. Additional translation results on two-domain datasets are presented in Fig. 12. Fig. 13 and Fig. 14 show synthesized results by the proposed SoloGAN for three-domain or four-domain datasets. For the translation task of *leopard* \leftrightarrow *lion* \leftrightarrow *tiger* \leftrightarrow *bobcat*, the stripes and dots of the translated leopards and tigers are different from each other (i.e., diverse translated images).

F. Limitations

Although the proposed SoloGAN model performs well in image translation for multiple domains, it is a data-driven approach and thus limited by the images in the training set (e.g., number of images and pose). left. For example, as there are no images in *cat* dataset with the same head pose as the tiger, the SoloGAN method fails to translate images in the target domain, as shown in Fig. 15(a). Similarly, the proposed method does not perform well when only a few training images of white horses are available (Fig. 15(b)).



Fig. 11: Example-guided image translations synthesized by the proposed SoloGAN model. Each row has the same content while each column has the same style.

V. CONCLUSION

We proposed a method for multimodal multi-domain image-to-image translation using a single pair of GANs. In the SoloGAN model, the content and style encoder as well as the generator are shared among multiple domains, and a projection with classification discriminator is proposed. Experimental results demonstrate that the SoloGAN model performs favorably in terms of both effectiveness and efficiency, especially for the translations tasks that involve complex image backgrounds or large shape changes.

REFERENCES

- [1] X. Huang, M.-Y. Liu, S. Belongie, and J. Kautz, “Multimodal unsupervised image-to-image translation,” in *Proceedings of the European Conference on Computer Vision*, 2018, pp. 172–189. 1, 2, 3, 4, 5, 6, 8

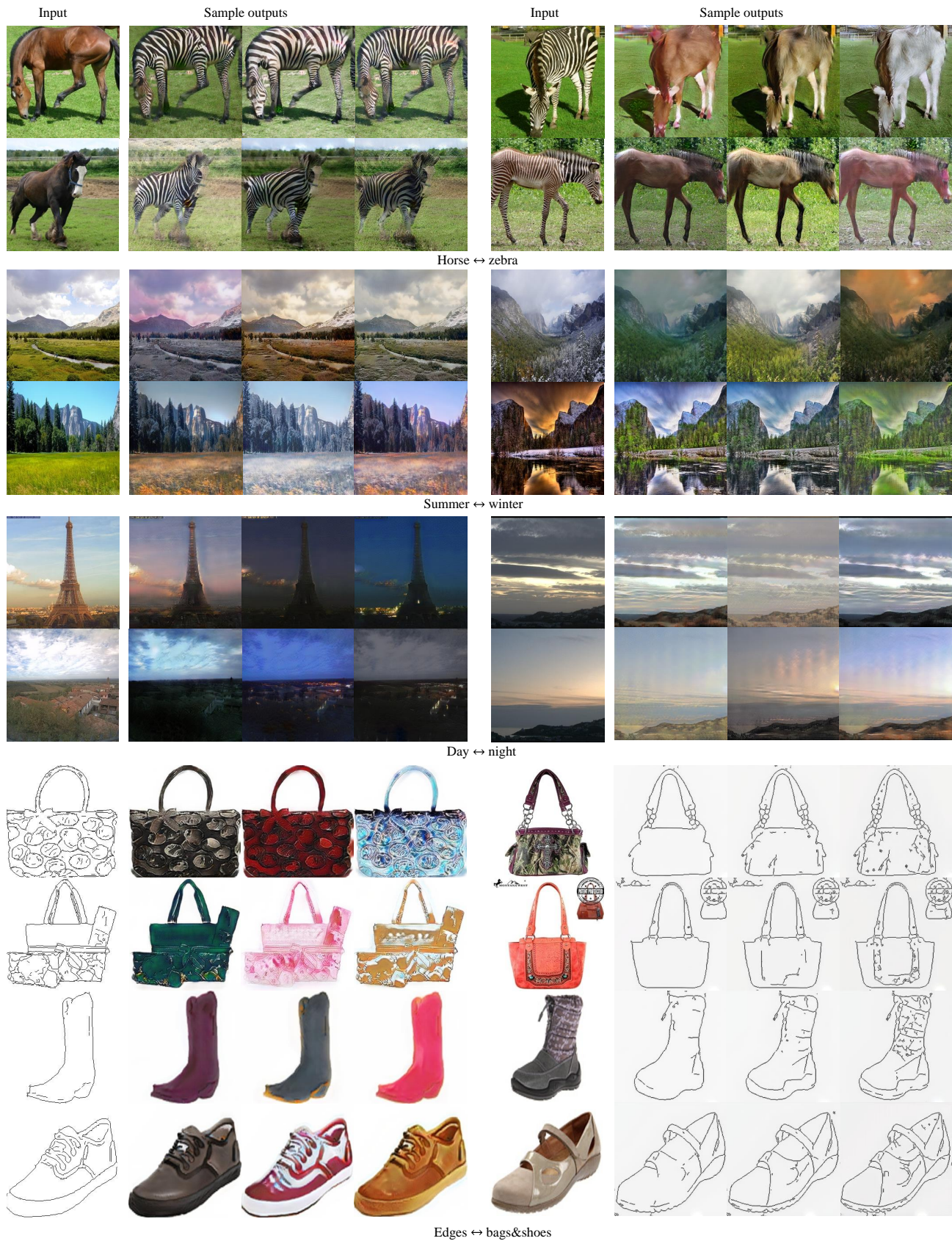


Fig. 12: Translated results on two-domain datasets. We train the SoloGAN over *edges* \leftrightarrow *bags&shoes* with 60 epochs.

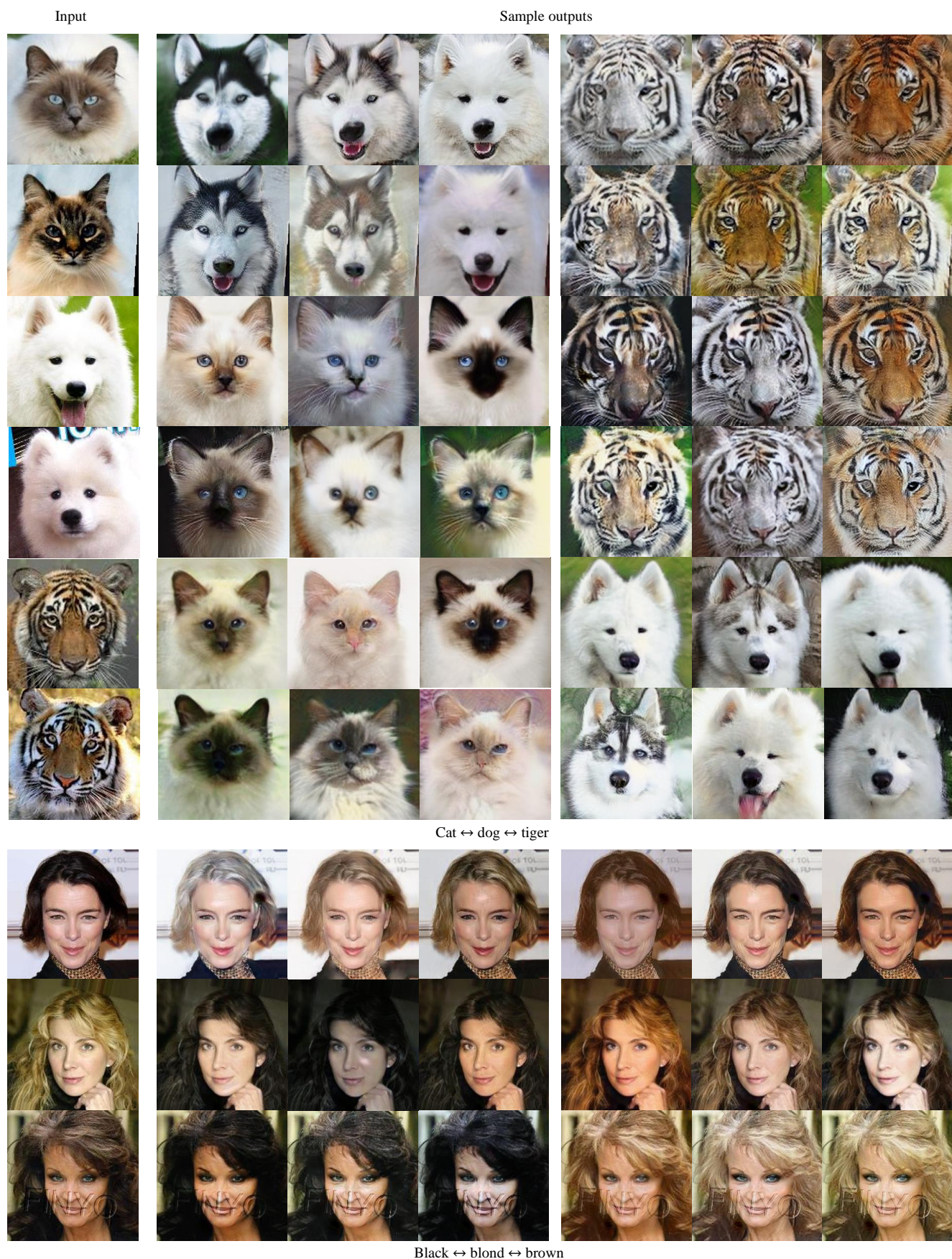


Fig. 13: Translated results on three-domain datasets. The SoloGAN is trained with 60 epochs over *black* \leftrightarrow *blond* \leftrightarrow *brown*.

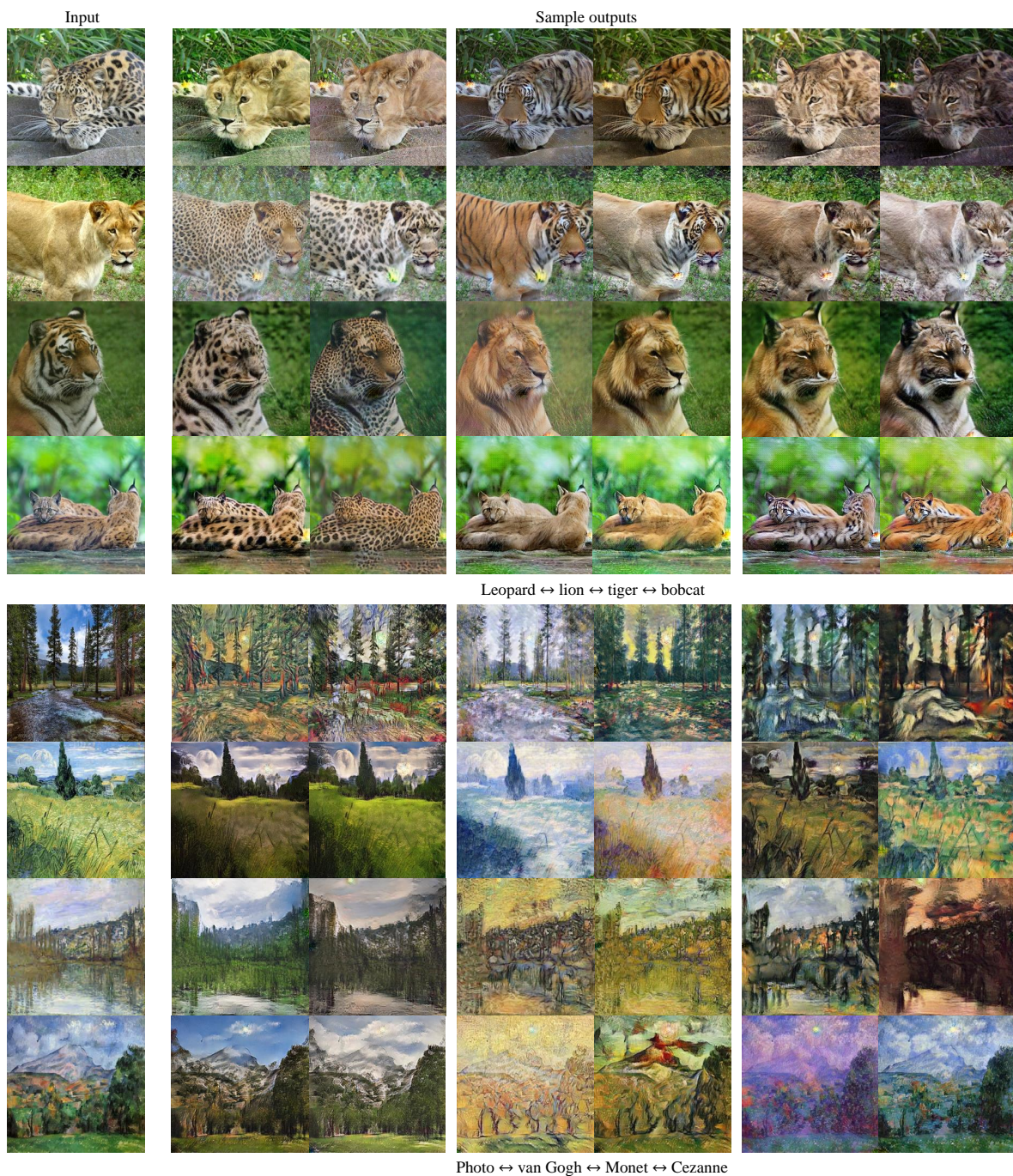


Fig. 14: Translated results on four-domain datasets.

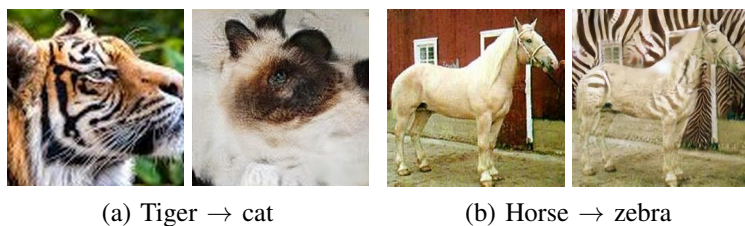


Fig. 15: Typical failure cases of the proposed SoloGAN.

- [2] H.-Y. Lee, H.-Y. Tseng, J.-B. Huang, M. Singh, and M.-H. Yang, "Diverse image-to-image translation via disentangled representations," *arXiv preprint arXiv:1808.00948*, 2018. 1, 2, 3, 4, 5, 6, 8
- [3] I. Goodfellow, J. Pouget-Abadie, M. Mirza, B. Xu, D. Warde-Farley, S. Ozair, A. Courville, and Y. Bengio, "Generative adversarial nets," in *Advances in Neural Information Processing Systems*, 2014, pp. 2672–2680. 1, 3
- [4] W. Deng, L. Zheng, Q. Ye, G. Kang, Y. Yang, and J. Jiao, "Image-image domain adaptation with preserved self-similarity and domain-dissimilarity for person re-identification," in *Proceedings of the IEEE Conference on Computer Vision and Pattern Recognition*, 2018, pp. 994–1003. 1
- [5] Y. Huang, J. Xu, Q. Wu, Z. Zheng, Z. Zhang, and J. Zhang, "Multi-pseudo regularized label for generated data in person re-identification," *IEEE Transactions on Image Processing*, vol. 28, no. 3, pp. 1391–1403, 2018. 1
- [6] C. Ledig, L. Theis, F. Huszár, J. Caballero, A. Cunningham, A. Acosta, A. P. Aitken, A. Tejani, J. Totz, Z. Wang *et al.*, "Photo-realistic single image super-resolution using a generative adversarial network," in *Proceedings of the IEEE Conference on Computer Vision and Pattern Recognition*, 2017, pp. 4681–4690. 1
- [7] A. Lucas, S. Lopez-Tapia, R. Molina, and A. K. Katsaggelos, "Generative adversarial networks and perceptual losses for video super-resolution," *IEEE Transactions on Image Processing*, vol. 28, no. 7, pp. 3312–3327, 2019. 1
- [8] H. Zhang, T. Xu, H. Li, S. Zhang, X. Wang, X. Huang, and D. N. Metaxas, "StackGAN: Text to photo-realistic image synthesis with stacked generative adversarial networks," in *Proceedings of the IEEE International Conference on Computer Vision*, 2017, pp. 5907–5915. 1
- [9] T. Xu, P. Zhang, Q. Huang, H. Zhang, Z. Gan, X. Huang, and X. He, "AttnGAN: Fine-grained text to image generation with attentional generative adversarial networks," in *Proceedings of the IEEE Conference on Computer Vision and Pattern Recognition*, 2018, pp. 1316–1324. 1
- [10] Z. He, W. Zuo, M. Kan, S. Shan, and X. Chen, "AttGAN: Facial attribute editing by only changing what you want," *IEEE Transactions on Image Processing*, 2019. 1
- [11] A. Pumarola, A. Agudo, A. M. Martinez, A. Sanfeliu, and F. Moreno-Noguer, "Ganimation: Anatomically-aware facial animation from a single image," in *Proceedings of the European Conference on Computer Vision*, 2018, pp. 818–833. 1, 3
- [12] Y. Choi, M. Choi, M. Kim, J.-W. Ha, S. Kim, and J. Choo, "Stargan: Unified generative adversarial networks for multi-domain image-to-image translation," in *Proceedings of the IEEE Conference on Computer Vision and Pattern Recognition*, 2018, pp. 8789–8797. 1, 2, 3, 6
- [13] P. Isola, J.-Y. Zhu, T. Zhou, and A. A. Efros, "Image-to-image translation with conditional adversarial networks," in *Proceedings of the IEEE Conference on Computer Vision and Pattern Recognition*, 2017, pp. 1125–1134. 1, 2, 3, 6
- [14] X. Chen, C. Xu, X. Yang, L. Song, and D. Tao, "Gated-GAN: Adversarial gated networks for multi-collection style transfer," *IEEE Transactions on Image Processing*, vol. 28, no. 2, pp. 546–560, 2018. 1
- [15] Y. Li, S. Tang, R. Zhang, Y. Zhang, J. Li, and S. Yan, "Asymmetric gan for unpaired image-to-image translation," *IEEE Transactions on Image Processing*, 2019. 1
- [16] C. Wang, C. Xu, C. Wang, and D. Tao, "Perceptual adversarial networks for image-to-image transformation," *IEEE Transactions on Image Processing*, vol. 27, no. 8, pp. 4066–4079, 2018. 1
- [17] C. Yang, T. Kim, R. Wang, H. Peng, and C.-C. J. Kuo, "Show, attend and translate: Unsupervised image translation with self-regularization and attention," *IEEE Transactions on Image Processing*, 2019. 1
- [18] T. Kim, M. Cha, H. Kim, J. K. Lee, and J. Kim, "Learning to discover cross-domain relations with generative adversarial networks," *arXiv preprint arXiv:1703.05192*, 2017. 1
- [19] Z. Yi, H. Zhang, P. Tan, and M. Gong, "DualGAN: Unsupervised dual learning for image-to-image translation," in *Proceedings of the IEEE International Conference on Computer Vision*, 2017, pp. 2849–2857. 1
- [20] J.-Y. Zhu, T. Park, P. Isola, and A. A. Efros, "Unpaired image-to-image translation using cycle-consistent adversarial networks," in *Proceedings of the IEEE International Conference on Computer Vision*, 2017, pp. 2223–2232. 1, 2, 3, 4, 6
- [21] M.-Y. Liu, T. Breuel, and J. Kautz, "Unsupervised image-to-image translation networks," in *Advances in Neural Information Processing Systems*, 2017, pp. 700–708. 1
- [22] J.-Y. Zhu, R. Zhang, D. Pathak, T. Darrell, A. A. Efros, O. Wang, and E. Shechtman, "Toward multimodal image-to-image translation," in *Advances in Neural Information Processing Systems*, 2017, pp. 465–476. 1, 2, 3, 5
- [23] T. Miyato and M. Koyama, "cGANs with projection discriminator," *arXiv preprint arXiv:1802.05637*, 2018. 1, 3
- [24] X. Yu, X. Cai, Z. Ying, T. Li, and G. Li, "SingleGAN: Image-to-image translation by a single-generator network using multiple generative adversarial learning," *arXiv preprint arXiv:1810.04991*, 2018. 2, 3, 6, 8
- [25] M. Heusel, H. Ramsauer, T. Unterthiner, B. Nessler, and S. Hochreiter, "GANs trained by a two time-scale update rule converge to a local nash equilibrium," in *Advances in Neural Information Processing Systems*, 2017, pp. 6626–6637. 2, 6
- [26] X. Mao, Q. Li, H. Xie, R. Y. Lau, Z. Wang, and S. P. Smolley, "Least squares generative adversarial networks," in *Proceedings of the IEEE International Conference on Computer Vision*, 2017, pp. 2794–2802. 3, 4
- [27] I. Gulrajani, F. Ahmed, M. Arjovsky, V. Dumoulin, and A. C. Courville, "Improved training of Wasserstein GANs," in *Advances in Neural Information Processing Systems*, 2017, pp. 5767–5777. 3
- [28] T. Salimans and D. P. Kingma, "Weight normalization: A simple reparameterization to accelerate training of deep neural networks," in *Advances in Neural Information Processing Systems*, 2016, pp. 901–909. 3
- [29] T. Miyato, T. Kataoka, M. Koyama, and Y. Yoshida, "Spectral normalization for generative adversarial networks," *arXiv preprint arXiv:1802.05957*, 2018. 3, 5
- [30] M. Mirza and S. Osindero, "Conditional generative adversarial nets," *arXiv preprint arXiv:1411.1784*, 2014. 3
- [31] A. Odena, C. Olah, and J. Shlens, "Conditional image synthesis with auxiliary classifier gans," in *Proceedings of the International Conference on Machine Learning-Volume*. JMLR. org, 2017, pp. 2642–2651. 3
- [32] A. Hertzmann, C. E. Jacobs, N. Oliver, B. Curless, and D. H. Salesin, "Image analogies," in *Proceedings of the 28th Annual Conference on Computer Graphics and Interactive Techniques*, 2001, pp. 327–340. 3
- [33] A. Anosheh, E. Agustsson, R. Timofte, and L. Van Gool, "Combogan: Unrestrained scalability for image domain translation," in *Proceedings of the IEEE Conference on Computer Vision and Pattern Recognition Workshops*, 2018, pp. 783–790. 3
- [34] X. Yu, Z. Ying, G. Li, and W. Gao, "Multi-mapping image-to-image translation with central biasing normalization," *arXiv preprint arXiv:1806.10050*, 2018. 3
- [35] H. Zhang, I. Goodfellow, D. Metaxas, and A. Odena, "Self-attention generative adversarial networks," *arXiv preprint arXiv:1805.08318*, 2018. 3
- [36] A. Brock, J. Donahue, and K. Simonyan, "Large scale gan training for high fidelity natural image synthesis," *arXiv preprint arXiv:1809.11096*, 2018. 3
- [37] T.-C. Wang, M.-Y. Liu, J.-Y. Zhu, A. Tao, J. Kautz, and B. Catanzaro, "High-resolution image synthesis and semantic manipulation with conditional GANs," in *Proceedings of the IEEE Conference on Computer Vision and Pattern Recognition*, 2018, pp. 8798–8807. 4
- [38] D. P. Kingma and J. Ba, "Adam: A method for stochastic optimization," *arXiv preprint arXiv:1412.6980*, 2014. 5
- [39] P.-Y. Laffont, Z. Ren, X. Tao, C. Qian, and J. Hays, "Transient attributes for high-level understanding and editing of outdoor scenes," *ACM Transactions on Graphics*, vol. 33, no. 4, p. 149, 2014. 6
- [40] C. H. Lampert, H. Nickisch, and S. Harmeling, "Learning to detect unseen object classes by between-class attribute transfer," in *Proceedings of the IEEE Conference on Computer Vision and Pattern Recognition*, 2009, pp. 951–958. 6
- [41] Z. Liu, P. Luo, X. Wang, and X. Tang, "Large-scale celebfaces attributes CelebA dataset," *Retrieved August*, vol. 15, p. 2018, 2018. 6
- [42] T. Salimans, I. Goodfellow, W. Zaremba, V. Cheung, A. Radford, and X. Chen, "Improved techniques for training gans," in *Advances in Neural Information Processing Systems*, 2016, pp. 2234–2242. 6
- [43] C. Szegedy, V. Vanhoucke, S. Ioffe, J. Shlens, and Z. Wojna, "Rethinking the inception architecture for computer vision," in *Proceedings of the IEEE Conference on Computer Vision and Pattern Recognition*, 2016, pp. 2818–2826. 6
- [44] R. Zhang, P. Isola, A. A. Efros, E. Shechtman, and O. Wang, "The unreasonable effectiveness of deep features as a perceptual metric," in *Proceedings of the IEEE Conference on Computer Vision and Pattern Recognition*, 2018, pp. 586–595. 6
- [45] A. Krizhevsky, I. Sutskever, and G. E. Hinton, "Imagenet classification with deep convolutional neural networks," in *Advances in Neural Information Processing Systems*, 2012, pp. 1097–1105. 6